Revisiting $B \to K^*(\to K\pi)\nu\bar{\nu}$ decays

Diganta Das,[1,*] Gudrun Hiller,[2,†] and Ivan Nišandžić[2,‡]

[1]*Physical Research Laboratory, Navrangpura, Ahmedabad 380 009, India*
[2]*Institut für Physik, Technische Universität Dortmund, D-44221 Dortmund, Germany*

The rare decay $B \to K^*(\to K\pi)\nu\bar{\nu}$ is expected to play an important role in searches for physics beyond the Standard Model at the near future B-physics experiments. We investigate resonant and nonresonant backgrounds that arise beyond the narrow-width approximation for the K^*. Nonresonant $B \to K\pi\nu\bar{\nu}$ decays are analyzed in the region of low hadronic recoil, where $B \to K\pi$ form factors from the heavy-hadron-chiral-perturbation theory are available. In a Breit-Wigner–type model interference-induced effects in the K^* signal region are found to be sizable, as large as 20% in the branching ratio. Corresponding effects in the longitudinal polarization fraction F_L are smaller, at most around a few percent. Effects of the broad scalar states K_0^* and κ are at the level of percent in the branching fraction in the K^* signal region and negligible in F_L. Since the backgrounds to F_L are small, this observable constitutes a useful probe of form factor calculations or, alternatively, of right-handed currents in the entire q^2 region. The forward-backward asymmetry in the $K\pi$ system, $A_{\mathrm{FB}\,L}^K$, with normalization to the longitudinal decay rate probes predominantly S, P-wave interference free of short-distance coefficients and can therefore be used to control the resonant and nonresonant backgrounds.

I. INTRODUCTION

The rare semileptonic hadron decays induced by $|\Delta B| = |\Delta S| = 1$ flavor changing neutral currents are sensitive probes of the Standard Model (SM) and beyond. The transitions $b \to s\ell^+\ell^-$, where $\ell = e$, μ, have been the subject of extensive theoretical and experimental studies in the past several decades [1,2]. The main theoretical challenges for the reliable extraction of Wilson coefficients from the experimental data arise from the requirement of the quantitative understanding of QCD backgrounds at large distances. To test the SM and to improve the understanding of theoretical uncertainties one can pursue studies with $b \to s\nu\bar{\nu}$ transitions, which are related by $SU(2)_L$ to $b \to s\ell^+\ell^-$ but not being subjected to sizable electromagnetic contributions from charm quarks. While dineutrino modes are theoretically better understood, they are experimentally more challenging and have not been observed to date. One can expect, however, that exclusive dineutrino modes with SM branching ratios of $\sim 10^{-5}$ will be observed and probed at the forthcoming Belle II experiment [3,4]. The current best limit is from the Belle Collaboration and reads, at 90% confidence level [5],

$$\mathcal{B}(B \to K^{*0}\bar{\nu}\nu) < 1.8 \times 10^{-5}, \tag{1}$$

which is just around the corner of the SM prediction. Dedicated studies of the impact of new physics on $b \to s\nu\bar{\nu}$

*diganta@prl.res.in
†ghiller@physik.uni-dortmund.de
‡ivan.nisandzic@tu-dortmund.de

processes can be found in the recent literature [6–10]; see also [11,12]. Here we focus on $B^0 \to K^{0*}(\to K\pi)\nu\bar{\nu}$ decays and analyze the interplay of the SM induced backgrounds for a K^* meson beyond the narrow-width approximation (NWA). Corresponding effects in $B \to K^*(\to K\pi)\ell^+\ell^-$ decays from scalar states and nonresonant contributions have been investigated previously in [13–15] and [16,17], respectively. Interestingly, the S-wave fraction in $B \to K^*(\to K\pi)\mu^+\mu^-$ has recently been measured by the LHCb Collaboration [18].

We consider only decays of neutral B mesons and omit the charge indices throughout; the corresponding decays of charged B mesons are additionally impacted by tree level charged currents via a resonant tau lepton [19].

After setting the notation in Sec. II A, we give amplitudes and distributions for an asymptotic final state K^* in Sec. II B. In Sec. III we work out effects from intermediate scalar mesons K_0^* and κ, which contribute to the creation of the outgoing $K\pi$ pair beyond the NWA for K^*. Nonresonant $B \to K\pi\nu\bar{\nu}$ contributions for a $K\pi$ mass around the one of the K^* are analyzed in Sec. IV. In Sec. V we conclude. Auxiliary information is deferred to three appendixes.

II. GENERALITIES

We give the effective $b \to s\nu\bar{\nu}$ Hamiltonian used in this work and some notation in Sec. II A and $B \to K^*\nu\bar{\nu}$ distributions for a zero-width K^* in Sec. II B.

A. Effective Hamiltonian and notation

We begin with the low energy effective Hamiltonian for $b \to s\nu\bar{\nu}$ transitions following [6,8]

$$\mathcal{H}_{\text{eff}} = -\frac{4G_F}{\sqrt{2}}\lambda_t \frac{\alpha}{8\pi}[(C_L + C_R)(\bar{s}\gamma_\mu b)$$
$$+ (C_R - C_L)(\bar{s}\gamma_\mu\gamma_5 b)]\sum_i \bar{\nu}_i\gamma^\mu(1 - \gamma_5)\nu_i + \text{H.c.},$$

$$(2)$$

where $\lambda_t = V_{tb}V_{ts}^*$ is the product of the Cabibbo-Kobayashi-Maskawa (CKM) matrix elements and α is the electromagnetic coupling constant. The ν_i denotes the neutrinos with flavors $i = e, \mu, \tau$. The value of the Wilson coefficient C_L within the SM was calculated at the next-to-leading order in QCD [20–22]. It is given by $C_L = -X(x_t)/\sin^2\theta_W$, where $x_t = m_t^2/m_W^2$ and $X(x_i)$ is the corresponding loop function with $X(x_t) = 1.469 \pm 0.017$ [11]. The right-handed Wilson coefficient C_R is negligible within the SM, but can be induced in beyond the SM (BSM) scenarios. We therefore keep the explicit dependence on this coefficient in the analytical expressions.

We denote the four-momenta of the B, K^*, K, and π mesons by p_B, k, p_K, and p_π, respectively, while the four-momenta of the neutrino and the antineutrino are denoted by p_ν and $p_{\bar{\nu}}$. We use $q = p_\nu + p_{\bar{\nu}}$ and $p = p_K + p_\pi$. m_X denotes the mass of the meson $X = B, K^*, K, \pi$. The polarization vectors of the K^* meson and the neutrino pair in the rest frame of the B meson are given in Appendix A.

B. $B \to K^*\nu\bar{\nu}$

We recall the expressions for the $B \to K^*\nu\bar{\nu}$ decay amplitude and differential decay rate for an asymptotic K^*-meson state. The amplitude for $B \to K^*\nu_i\bar{\nu}_i$ decays, with fixed K^* polarization $n = \pm, 0$, can be written as

$$\mathcal{A}(n) = -\frac{4G_F}{\sqrt{2}}\lambda_t\frac{\alpha}{8\pi}h_\mu(n)\ell^\mu, \qquad (3)$$

where

$$h_\mu(n) = (C_L + C_R)\langle K^*(n)|\bar{s}\gamma_\mu b|B\rangle$$
$$+ (C_R - C_L)\langle K^*(n)|\bar{s}\gamma_\mu\gamma_5 b|B\rangle, \qquad (4)$$

and ℓ^μ denotes the matrix element of the vector-minus-axial neutrino current between the vacuum and the neutrino pair. The matrix elements of the vector and axial-vector currents between the B and K^* mesons are parametrized in terms of the standard form factors, explicitly given in Appendix B. We use the $B \to K^*$ form factors given in Ref. [23], which were obtained from a combined fit [24] of lattice QCD [25] and light-cone sum rules (LCSR) results [23].

The hadronic amplitudes h_μ are written in terms of the hadronic helicity amplitudes H, which are defined as projections of the hadronic matrix onto the polarization vectors of the neutrino pair for a given K^* polarization n as

$$H_n = \tilde{\epsilon}_n^{\mu*}h_\mu(n), \qquad n = \pm, 0. \qquad (5)$$

For easier comparison with the literature, we switch to the transversity basis of perpendicular ($\perp$) and parallel ($\parallel$) polarizations via $H_\perp = 1/\sqrt{2}(H_+ - H_-)$ and $H_\parallel = 1/\sqrt{2}(H_+ + H_-)$, while the H_0 remains unchanged from Eq. (5). The hadronic transversity amplitudes then read

$$H_\perp(q^2) = \frac{\sqrt{2}(C_L + C_R)\lambda^{1/2}(m_B^2, q^2, m_{K^*}^2)}{m_B + m_{K^*}}V(q^2),$$

$$H_\parallel(q^2) = \sqrt{2}(C_L - C_R)(m_B + m_{K^*})A_1(q^2),$$

$$H_0(q^2) = -\frac{1}{2m_{K^*}\sqrt{q^2}}(C_L - C_R)$$
$$\times \left[(m_B + m_{K^*})(m_B^2 - m_{K^*}^2 - q^2)A_1(q^2)\right.$$
$$\left. - \frac{\lambda(m_B^2, q^2, m_{K^*}^2)}{m_B + m_{K^*}}A_2(q^2)\right], \qquad (6)$$

TABLE I. SM branching fractions in units of 10^{-6} for different cuts in p^2 [see (25)] and q^2 as indicated. The (first) row with $B \to K^*\bar{\nu}\nu$ corresponds to the NWA, while in the second and third rows finite width effects (10) of the K^* have been included. The ranges given for the scalar resonance contributions correspond to the ranges of the scalar form factors (B4) and the parameters in (11). Interference between the scalar- and vector-meson induced amplitudes is lost upon $\cos\theta_K$ integration such that the corresponding branching fractions can simply be added. The second uncertainty in the last two rows stems mostly from the unknown strong phase δ. The symbol $\cdots$ indicates that theoretical predictions are not available; see text for details.

	Low $q^2 \in [0\text{–}14]$ GeV^2	High $q^2 \in [14\text{–}19]$ GeV^2
$\mathcal{B}(B \to K^*\nu\bar{\nu})|_{\text{NWA}}$	6.96 ± 0.76	2.50 ± 0.22
$\mathcal{B}(B \to K^*(\to K\pi)\nu\bar{\nu})|_{P\text{-cut}}$	6.01 ± 0.65	2.09 ± 0.22
$\mathcal{B}(B \to K^*(\to K\pi)\nu\bar{\nu})|_{S+P\text{-cut}}$	6.80 ± 0.73	2.29 ± 0.23
$\mathcal{B}(B \to (\kappa, K_0^*)(\to K\pi)\nu\bar{\nu})|_{P\text{-cut}}$	$[0.01\cdots0.07]$	$\cdots$
$\mathcal{B}(B \to (\kappa, K_0^*)(\to K\pi)\nu\bar{\nu})|_{S+P\text{-cut}}$	$[0.04\cdots0.30]$	$\cdots$
$\mathcal{B}(B \to (K^* + \text{nonres})(\to K\pi)\nu\bar{\nu})|_{P\text{-cut}}$	$\cdots$	$2.09 \pm 0.22^{+0.42}_{-0.29}$
$\mathcal{B}(B \to (K^* + \text{nonres})(\to K\pi)\nu\bar{\nu})|_{S+P\text{-cut}}$	$\cdots$	$2.29 \pm 0.23^{+0.62}_{-0.27}$

where $\lambda(a, b, c) = a^2 + b^2 + c^2 - 2(ab + bc + ca)$. The differential decay distribution in q^2, the square of the invariant mass of the $\nu\bar{\nu}$ pair, is then given as

$$\frac{d\Gamma}{dq^2} = 3\frac{G_F^2|\lambda_t|^2\alpha^2|\vec{q}|q^2}{128 \times 3\pi^5 m_B^2}[|H_\perp|^2 + |H_\parallel|^2 + |H_0|^2], \quad (7)$$

with $|\vec{q}| = \lambda^{1/2}(m_B^2, m_{K^*}^2, q^2)/(2m_B)$. Here, the overall factor of 3 comes from the summation over three flavors of the final state neutrinos. Formula (7) agrees with the corresponding results in [6,8]. Integrating this distribution over the full kinematic region $0 \leq q^2 \leq (m_B - m_{K^*})^2$ we obtain for the SM branching ratio

$$\mathcal{B}(B \to K^*\bar{\nu}\nu) = (9.49 \pm 1.01) \times 10^{-6}, \quad (8)$$

consistent with [7,10,11]. Partial branching ratios in low and high q^2 regions are given in Table I; see Sec. III B for the definition of our current choice of binning in q^2.

Separate q^2 regions are needed since form factors for the background modes $B \to K_0^*(\to K\pi)\nu\bar{\nu}$ and $B \to K\pi\nu\bar{\nu}$ are presently not available in the full q^2 region.

III. RESONANT CONTRIBUTIONS $B \to K_{res}(\to K\pi)\nu\bar{\nu}$

In this section we treat the K^* at finite width and include intermediate scalar states decaying as well to $K\pi$. Such effects have been studied previously for $B \to K^*\ell^+\ell^-$ decays [13–15] and measured recently by the LHCb Collaboration [18]. In Sec. III A we obtain decay amplitudes and distributions for $B \to (K^*, K_0^*, \kappa)(\to K\pi)\nu\bar{\nu}$ decays. In Sec. III B we work out their phenomenology.

A. Amplitudes and observables

The total, resonant amplitude with fixed polarization n of the final $K\pi$ pair can be written as

$$\mathcal{A}(B \to K_{res}(n)(\to K\pi)\bar{\nu}_i\nu_i) = -\frac{4G_F}{\sqrt{2}}\lambda_t\frac{\alpha}{8\pi}\sum_{res}\langle K\pi|K_{res}(n)\rangle[(C_L + C_R)\langle K_{res}(n)|\bar{s}\gamma_\mu b|B\rangle$$
$$+ (C_R - C_L)\langle K_{res}(n)|\bar{s}\gamma_\mu\gamma_5 b|B\rangle]\ell^\mu\widetilde{BW}_{res}(p^2), \quad (9)$$

where $p^2 = (p_K + p_\pi)^2$ denotes the square of the invariant mass of the $K\pi$ pair. We parametrize the propagator of the intermediate vector K^* resonance by a Breit-Wigner ansatz

$$\widetilde{BW}_{K^*}(p^2) = \frac{1}{p^2 - m_{K^*}^2 + im_{K^*}\Gamma_{K^*}}, \quad (10)$$

where Γ_{K^*} denotes the (constant) width of the K^* [26]. In the absence of $B \to K^*$ form factors that take into account the finite width of the K^* we employ the available narrow-width ones instead.

For the broad scalar states we follow Ref. [13] and include the contribution of the $K_0^*(800) \equiv \kappa$ that modifies the tail of the $K_0^*(1430)$ resonance in the p^2-region relevant to the K^*,

$$\widetilde{BW}_{scalar}(p^2) = -\frac{g_\kappa}{p^2 - (m_\kappa - i\Gamma_\kappa/2)^2}$$
$$+ \frac{1}{p^2 - (m_{K_0^*} - i\Gamma_{K_0^*}/2)^2}. \quad (11)$$

We employ the mass and the width of the scalar state κ from Ref. [27], and the ranges of the magnitude and argument of g_κ given in [13], which are compatible with $D \to K^*\ell\nu$ spectra [13,28]; see Table III for a compilation of numerical input used in this work. For alternative descriptions, see [29,30] and [16]. We checked explicitly that the model (11)

is consistent with the measurements of the scalar fraction F_S and the $\cos\theta_K$ distribution in $B \to K^*(\to K\pi)\mu^+\mu^-$ decays [18] and the p^2 distribution near the K^* [31]. In the future experimental checks can be explicitly performed directly for the dineutrino mode by measuring the interference observable b; see (18). As for the K^* we neglect a possible p^2 dependence in the decay widths.

The $K^*, K_0^* \to K\pi$ decay amplitudes are expressed in terms of the couplings $g_{K^*K\pi}$ and $g_{K_0^*K\pi}$, defined as

$$\langle K^i(p_K)\pi^j(p_\pi)|K^*(k, n)\rangle = c_{ij}(\epsilon_n \cdot p_K)g_{K^*K\pi},$$
$$\langle K^i(p_K)\pi^j(p_\pi)|K_0^*(k)\rangle = c_{ij}g_{K_0^*K\pi}. \quad (12)$$

Here, c_{ij} denote isospin factors that depend on the charges of the final state mesons, i.e., $|c_{+-}| = \sqrt{2}|c_{00}| = 1$. The magnitudes of the couplings can be obtained from the corresponding decay rates using

$$\Gamma(K^* \to K^i\pi^j) = \frac{|c_{ij}|^2}{24\pi m_{K^*}^2}g_{K^*K\pi}^2|\vec{p}_K|^3,$$
$$\Gamma(K_0^* \to K^i\pi^j) = \frac{|c_{ij}|^2}{8\pi m_{K_0^*}^2}g_{K_0^*K\pi}^2|\vec{p}_K|, \quad (13)$$

where $|\vec{p}_K| = \lambda^{1/2}(m_{K_{(0)}^*}^2, m_K^2, m_\pi^2)/2m_{K_{(0)}^*}$. These couplings are important for the understanding of nonperturbative

strong interactions; $g_{K^*K\pi}$ has been computed in lattice QCD [32], consistent with data [26].

We write the amplitude for the $K^* \to K\pi$ transition in the $K\pi$ rest frame using the components of the kaon's four-momentum, that is, for the coordinate system defined in Appendix A, given by $p_K^\mu = (E_K, 0, |\vec{p}_K|\sin\theta_K, |\vec{p}_K|\cos\theta_K)$. We defined θ_K as the angle between the kaon and the opposite direction of the B meson in the $K\pi$ rest frame. The polarization vectors of the K^* resonance in this frame are $\epsilon_\pm^\mu = 1/\sqrt{2}(0, \pm 1, i, 0)$ and $\epsilon_0^\mu = (0, 0, 0, 1)$, resulting in $\epsilon_\pm \cdot p_K = -i\frac{1}{\sqrt{2}}|\vec{p}_K|\sin\theta_K$, $\epsilon_0 \cdot p_K = -|\vec{p}_K|\cos\theta_K$.

Using the projection (5) and the scalar form factor (B3), we obtain the corresponding hadronic helicity amplitude

$$H_0'(q^2) = (C_R - C_L)\frac{\lambda^{1/2}(m_B^2, q^2, m_{K_0^*}^2)}{\sqrt{q^2}} f_+(q^2). \quad (14)$$

For the form factor $f_+(q^2)$ we use the results of the QCD-sum-rules computation from Ref. [33]; see Appendix B.

To combine vector and scalar resonance effects we write the differential decay rate for the four-body final state process by introducing the helicity amplitudes, distinguished by the *tildae* labels, that incorporate, with the use of Eq. (12), the subsequent decay amplitude of the resonance into the final $K\pi$ pair, that is,

$$\tilde{H}_{\parallel,\perp}(q^2, p^2, \cos\theta) = -i\frac{1}{\sqrt{2}} g_{K^*K\pi}|\vec{p}_K'|\sin\theta_K \widetilde{BW}_{K^*}(p^2)$$
$$\times H_{\parallel,\perp}(q^2),$$

$$\tilde{H}_0(q^2, p^2, \cos\theta) = -g_{K^*K\pi}|\vec{p}_K'|\cos\theta_K \widetilde{BW}_{K^*}(p^2) H_0(q^2),$$

$$\tilde{H}_0'(q^2, p^2) = g_{K_0^*K\pi}\widetilde{BW}_{\text{scalar}}(p^2) H_0'(q^2), \quad (15)$$

where $|\vec{p}_K'|$ is defined in Eq. (17) below. Using the expression for the four-body phase space, e.g., [16,34], we obtain the threefold decay distribution

$$\frac{d^3\Gamma}{dq^2 dp^2 d\cos\theta_K}$$
$$= \frac{N(q^2)|\vec{q}'||\vec{p}_K'|}{8(2\pi)^5 m_B^2 \sqrt{p^2}}\left[\sum_{i=\parallel,\perp,0}|\tilde{H}_i|^2 + 2\mathcal{R}e(\tilde{H}_0\tilde{H}_0'^*) + |\tilde{H}_0'|^2\right],$$
$$(16)$$

with

$$N(q^2) = G_F^2\lambda_t^2\alpha^2 q^2/(8\pi^2),$$

$$|\vec{p}_K'| = \lambda^{1/2}(p^2, m_K^2, m_\pi^2)\Big/\left(2\sqrt{p^2}\right),$$

$$|\vec{q}'| = \lambda^{1/2}(m_B^2, p^2, q^2)/(2m_B). \quad (17)$$

Equation (7) is recovered in the NWA for the K^* after setting the scalar contributions to zero and integrating the above distribution over $\cos\theta_K$ in the interval $(-1, 1)$.

The threefold differential decay distribution (16) can be written as

$$\frac{d^2\Gamma}{dq^2 dp^2 d\cos\theta_K} = a(q^2, p^2) + b(q^2, p^2)\cos\theta_K$$
$$+ c(q^2, p^2)\cos^2\theta_K, \quad (18)$$

where, schematically,

$$a(q^2, p^2) \sim \sum_{i=\parallel,\perp}|\vec{p}_K|^2\frac{|H_i|^2}{2} + |H_0'|^2,$$

$$b(q^2, p^2)\cos\theta_K \sim -2|\vec{p}_K|\mathcal{R}e(H_0 H_0'^*),$$

$$c(q^2, p^2)\cos^2\theta_K \sim |\vec{p}_K|^2\left(|H_0|^2 - \sum_{i=\parallel,\perp}\frac{|H_i|^2}{2}\right). \quad (19)$$

The parametrization (18) is general for contributions from spin 0 and spin 1 kaon resonances. For spin ≥ 2 further powers of $\cos\theta_K$ arise. The coefficient functions $a(q^2, p^2), b(q^2, p^2), c(q^2, p^2)$ represent the three independent observables that can be measured in angular analysis in θ_K. Instead of a, b, c for phenomenology we consider the q^2-differential decay rate,[1]

$$\frac{d\Gamma}{dq^2} = 2\left(a(q^2) + \frac{c(q^2)}{3}\right), \quad (20)$$

and the longitudinal polarization fraction of the vector meson, F_L [8],

$$F_L = \frac{d\Gamma_L/dq^2}{d\Gamma/dq^2}, \qquad \frac{d\Gamma_L}{dq^2} = \frac{2}{3}(a(q^2) + c(q^2)), \quad (21)$$

both obtained after integration over p^2. As usual, the q^2-averaged (binned) versions of ratio-type observables are defined as

$$\langle F_L \rangle = \frac{\Gamma_L}{\Gamma}, \qquad \Gamma_{(L)} = \int_{q_{\min}^2}^{q_{\max}^2}\frac{d\Gamma_{(L)}}{dq^2}. \quad (22)$$

Note that F_L does not depend on the Wilson coefficients if right-handed currents can be neglected. In this case, which includes the SM and which may be checked elsewhere, F_L is probing form factors in the entire q^2 region. With a single observable it is not possible to extract two form factor ratios without further input. This is different in $B \to K^*\ell^+\ell^-$

---

[1]In what follows, a single argument implies that the other variable has been integrated over, e.g., $b(q^2) = \int dp^2 b(q^2, p^2)$ and $b(p^2) = \int dq^2 b(q^2, p^2)$, etc.
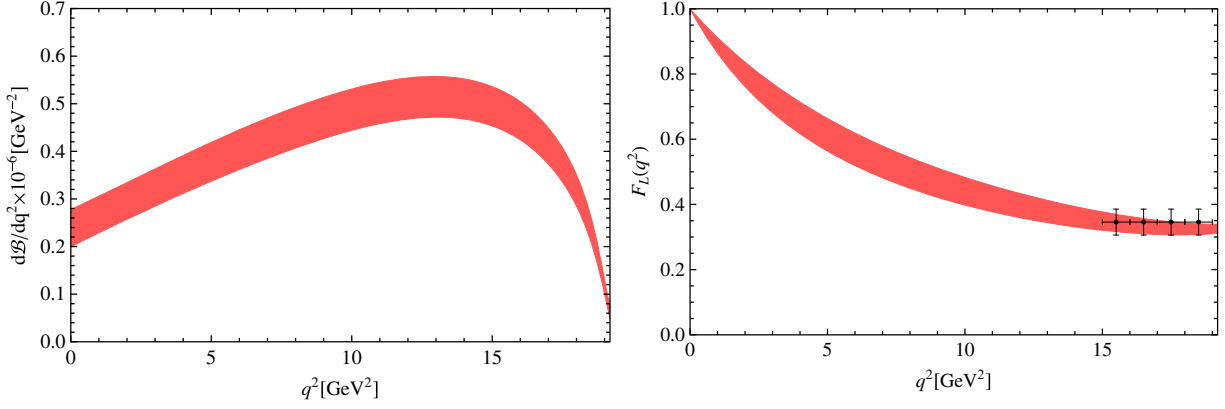
FIG. 1. Shown on the left is the differential SM branching fraction for the decay $B \to K^*(\to K\pi)\nu\bar{\nu}$ as the function of q^2, integrated over p^2 within the P cut; see (25). Shown on the right is the longitudinal polarization fraction $F_L(q^2)$. Here, the (black) data points correspond to form factor computations from lattice QCD [25,37]. The error bands result from the uncertainties in the form factors taken from a combined fit [23], and parametric inputs.

decays at high q^2 which allows for a fit [35]. Within the NWA for the K^* we find after integration over the full q^2 region

$$\langle F_L \rangle_{\mathrm{NWA}} = 0.49 \pm 0.04, \tag{23}$$

consistent with Ref. [8].

In addition, we consider the forward-backward asymmetry A_{FB}^K, or alternatively, $A_{\mathrm{FB\,L}}^K$,

$$A_{\mathrm{FB(L)}}^K \equiv \frac{\int_0^1 d\cos\theta_K \frac{d^2\Gamma}{dq^2 d\cos\theta_K} - \int_{-1}^0 d\cos\theta_K \frac{d^2\Gamma}{dq^2 d\cos\theta_K}}{\Gamma_{(L)}}$$

$$= \frac{b(q^2, p^2)}{\Gamma_{(L)}}, \tag{24}$$

induced by interference of the K^* with intermediate scalar states. It can be used to further check the size of the scalar background, as pointed out for $B \to K^*\ell^+\ell^-$ decays in Ref. [13]. By the same argument, $b = 0$ in the presence of vector K^* only. Note that contributions from $b(q^2, p^2)$ disappear from (18) after symmetric $\cos\theta_K$ integration. In the same way as in F_L the dependence on Wilson coefficients drops out in A_{FB}^K if right-handed currents are negligible. On the other hand, in $A_{\mathrm{FB\,L}}^K$ only amplitudes with $C_L - C_R$ enter, so the Wilson coefficients cancel in this ratio model independently.

B. Numerical analysis

We employ two different integration regions for p^2 [16,18],

$$[(m_{K^*} - 0.1 \text{ GeV})^2, (m_{K^*} + 0.1 \text{ GeV})^2] \qquad P \text{ cut}$$
$$[(m_K + m_\pi)^2, 1.44 \text{ GeV}^2] \qquad (S + P) \text{ cut}, \tag{25}$$

where the first one, termed P cut, refers to the K^* "P-wave" signal region. The second one, termed $S + P$ cut, refers to a wider region that allows one to study backgrounds, such as S-wave contributions.

After fixing the integration limits for p^2, the end point in q^2 is a function of p^2, that is, $q_{\mathrm{max}}^2 = (m_B - \sqrt{p^2})^2$. Note that some care is required with the comparison of the experimental results that follow from some choice of a finite integration region in p^2 with the result of Eq. (7). If one assumes the Breit-Wigner type parametrizations, as above, and applies the chosen p^2 cut, the differential decay rates over q^2 and the resulting total rates are smaller than those from Eq. (7). This can be explicitly seen from Table I and has also been pointed in Ref. [36] for $B_s \to K^*\ell\bar{\nu}$ decays.

We begin with the pure $B \to K^*(\to K\pi)\nu\bar{\nu}$ decays at finite width. In Fig. 1 we show the branching ratio and F_L in the SM as functions of q^2 in the signal (P-cut) window. Note that F_L goes to 1 and $1/3$ at maximal and zero recoil, respectively, as dictated by helicity. On top of the uncertainty bands from $B \to K^*$ form factors and parametric inputs we show for F_L exemplarily predictions from lattice form factors [25,37]. Recall that F_L is unaffected by BSM physics if C_R is negligible. As we will show, F_L in addition receives only small uncertainties from scalar and nonresonant backgrounds. We therefore suggest it as a probe of form factor calculations in the full q^2 region.

In the following it becomes necessary to separate the analysis into two q^2 regions, "low q^2" within the range [0–14] GeV^2 and "high q^2" within $q^2 \in$ [14–19] GeV^2. We refrain from presenting numerical predictions for intermediate scalar resonances at high q^2, where the extrapolation of the scalar form factors Eq. (B4) into the highly off-shell (for K_0^*) region is required. Instead, we find these effects to be highly subdominant in this region, their kinematic suppression toward the high q^2 region is evident
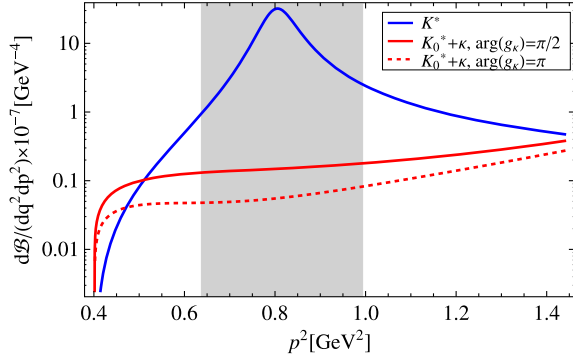
FIG. 2. Line shapes of the resonant K^* (10) (solid blue line) and scalar mesons [$K_0^*(1430)$, $\kappa(800)$] (red line) at $q^2 = 4$ GeV². All input parameters are set to their central values, and $g_\kappa = 0.2$, $\arg(g_\kappa) = \pi/2$ (red solid line) and $\arg(g_\kappa) = \pi$ (red dashed line); see Eq. (11). The (gray) shaded region corresponds to the P cut in p^2; cf. (25).

FIG. 3. The ratio of $B \to K^*(\to K\pi)\nu\bar{\nu}$ to $B \to (K^*, K_0^*, \kappa)$ $(\to K\pi)\nu\bar{\nu}$ q^2-differential branching ratios for different p^2 cuts. We set the $B \to K^*$ form factors and other inputs to their central values, except for the parameters which enter the scalar meson contributions [$B \to K_0^*$ form factors, g_κ, and other parameters in (11)]. We leave these parameters free within the corresponding errors, such that the boundaries of the above bands correspond to the resulting minimal and maximal values.

from Fig. 3. The other reason for a separation in q^2 is the nonresonant effects, whose description using chiral methods is expected to hold only at high q^2; see Sec. IV. The estimate of nonresonant effects in the low q^2 region is beyond the scope of this work.

The line shapes of the K^* and the scalars are shown in Fig. 2. They do not interfere in the $B \to (K^*, K_0^*, \kappa)$ $(\to K\pi)\nu\bar{\nu}$ differential branching ratio. Contributions from scalars underneath the K^* peak can be probed with sideband measurements or $A_{\mathrm{FB(L)}}^K$ (24).

The impact of the intermediate scalar meson states on $B \to K^*(\to K\pi)\nu\bar{\nu}$ is illustrated in Fig. 3. Shown is the ratio of $B \to K^*(\to K\pi)\nu\bar{\nu}$ to $B \to (K^*, K_0^*, \kappa)(\to K\pi)\nu\bar{\nu}$ differential branching ratios[2] for different p^2 cuts. After integrating over $\cos\theta_K$, the information on the interference between the scalar and vector amplitudes is lost and the corresponding branching fractions can simply be added. We find that the impact of the scalars drops with increasing q^2. It is at most $\sim 10\%$ for the $S + P$ cut and a few percent in the P cut.

After integrating over the low q^2 region the ratio between the corresponding integrated rates deviates from unity at the level of at most $\sim 1\%$ in the P cut and $\sim 4\%$ for the $(S + P)$ cut. Branching ratios involving only the K^* and only the scalars integrated over the low q^2 region are given in Table I. The ranges given for the scalars correspond to the minimal and maximal values obtained from the ranges of the scalar form factors [see Eq. (B4) and the text below] and parameters in (11).

For F_L we find that its value for pure $B \to K^*(\to K\pi)\nu\bar{\nu}$ decays does not differ between NWA, the P- and $(S + P)$-cut predictions at finite width. This can be expected since

the p^2 dependence is universal for all $\tilde{H}_i$; see Eq. (15). We also find that the effect of the scalar states on F_L is negligible compared to other sources of uncertainties. SM values for F_L are given in Table II.

In Fig. 4 we show the forward-backward asymmetry integrated over the low-q^2 region and normalized to the total rate in this region (left plot) and the total longitudinal rate (right plot), both integrated over p^2 in the $(S + P)$ cut. These observables can be used to test the model of the scalar contributions. The normalization to the longitudinal rate is particularly useful, since the Wilson coefficients $C_{L,R}$ drop out. $A_{\mathrm{FB(L)}}^K(p^2)$ change sign across p^2. Therefore, cancellations arise from integration over p^2 resulting in small values of $A_{\mathrm{FB(L)}}^K(q^2)$, of the order of a percent.

IV. NONRESONANT CONTRIBUTIONS

We consider nonresonant contributions to the four-body final state decay process. These contributions were studied in [38] and were recently taken into account in $B \to K^*\ell\ell$

---

[2]This ratio corresponds to $1 - F_S$, where F_S denotes the fraction of scalar contributions [15].

TABLE II. $\langle F_L \rangle$ in the SM for different cuts in p^2 [see (25)] and q^2 binning as indicated (see Table I). The entries in the first row are indistinguishable between the NWA and the finite width treatment (10) with P and $(S + P)$ cuts. The impact of scalar mesons is negligible. The last row gives $\langle F_L \rangle$ including nonresonant contributions.

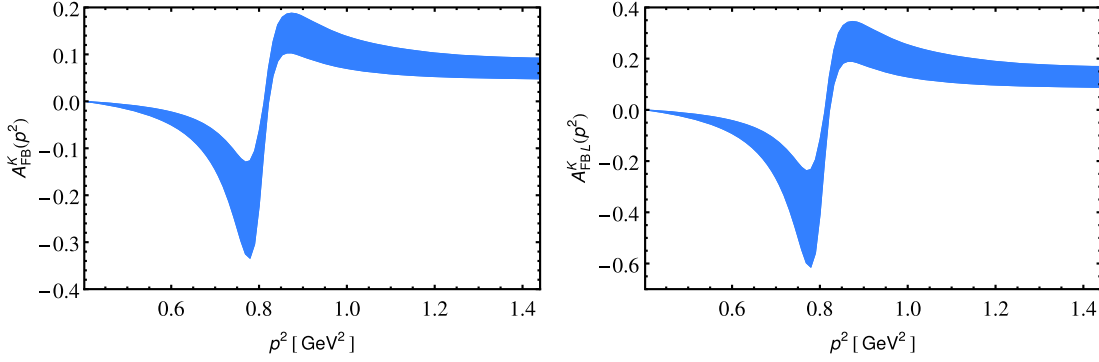|	Low $q^2 \in$ [0–14] GeV²	High $q^2 \in$ [14–19] GeV²
$\langle F_L \rangle\vert_{\mathrm{NWA},P-,(S+P)\text{-cut}}$	0.54 ± 0.04	0.34 ± 0.02
$\langle F_L \rangle(B \to (K^* + \mathrm{nonres})$ $(\to K\pi)\nu\bar{\nu})\vert_{P-,(S+P)\text{-cut}}$	$\cdots$	$0.34 \pm 0.02 \pm 0.01$

FIG. 4. The forward-backward asymmetry $A_{FB}^K(p^2)$ (plot to the left) and $A_{FB\,L}^K(p^2)$ (plot to the right) defined in (24) integrated over the low q^2 region. The corresponding decay rates have been integrated over the low q^2 region and the $(S+P)$ cut in p^2.

decays in [16,17], as well as some time ago in $D \to K\pi\ell\nu$ processes in [39]. The nonresonant matrix elements of the (axial-) vector currents between the B and the $K\pi$ can be parametrized as follows [38]:

$$\langle K^i\pi^j|\bar{s}\gamma_\mu b|B\rangle = c_{ij}h\epsilon_{\mu\nu\alpha\beta}p_B^\nu(p_K^\alpha + p_\pi^\alpha)(p_K^\beta - p_\pi^\beta),$$

$$\langle K\pi|\bar{s}\gamma_\mu\gamma_5 b|B\rangle = c_{ij}[-iw_+(p_{K\mu} + p_{\pi\mu})$$
$$- iw_-(p_{K\mu} - p_{\pi\mu}) - irq_\mu], \quad (26)$$

where the form factors $w_\pm$, h, and r are functions of q^2, p^2, and θ_K. They are presently not known from first principles of QCD. We use the leading order heavy-hadron-chiral-perturbation-theory (HHχPT) results [38,40]

$$w_\pm(q^2, p^2, \theta_K) = \pm \frac{gf_{B_d}}{2f^2}\frac{m_B}{v \cdot p_\pi + \Delta},$$

$$h(q^2, p^2, \theta_K) = \frac{g^2 f_{B_d}}{2f^2}\frac{1}{(v \cdot p_\pi + \Delta)(v \cdot p_{K\pi} + \Delta + \mu_s)}, \quad (27)$$

where v denotes the four-velocity of the B meson, $f^2 = f_\pi f_K$, $\Delta = m_{B^*} - m_B$, and $\mu_s = m_{B_s} - m_B$. We collect the corresponding numerical values of the inputs in Table III. The results in (27) are expected to be valid only in the kinematic range in which chiral perturbation theory applies. This corresponds to $p_B \cdot p_{\pi,K}/m_B \lesssim 1$ GeV, which is roughly satisfied in the high q^2 region.

The nonresonant $B \to K\pi\nu_i\bar{\nu}_i$ decay amplitude can be written as

$$\mathcal{A}(B \to K\pi\nu_i\bar{\nu}_i) = -\frac{4G_F}{\sqrt{2}}\lambda_t\frac{\alpha}{8\pi}[(C_L + C_R)\langle K\pi|\bar{s}\gamma_\mu b|B\rangle$$
$$+ (C_R - C_L)\langle K\pi|\bar{s}\gamma_\mu\gamma_5 b|B\rangle]\ell^\mu. \quad (28)$$

The nonresonant hadronic transversity amplitudes are obtained by projecting the matrix elements (26) onto the polarization vectors of the neutrino pair [see Eq. (5)],

$$H_\perp^{nr} = (C_L + C_R)\sin\theta_K\frac{\lambda^{1/2}(m_{K\pi}^2, m_K^2, m_\pi^2)\lambda^{1/2}(m_B^2, p^2, q^2)}{2\sqrt{p^2}}h,$$

$$H_\parallel^{nr} = -(C_L - C_R)\sin\theta_K\frac{\lambda^{1/2}(p^2, m_K^2, m_\pi^2)}{\sqrt{p^2}}w_-,$$

$$H_0^{nr} = \frac{i(C_L - C_R)}{2\sqrt{q^2}}\left[w_-\frac{1}{p^2}((m_K^2 - m_\pi^2)\lambda^{1/2}(m_B^2, q^2, p^2)\right.$$
$$- (m_B^2 - p^2 - q^2)\lambda^{1/2}(m_K^2, m_\pi^2, p^2)\cos\theta_K)$$
$$\left. + w_+\lambda^{1/2}(m_B^2, q^2, p^2)\right]. \quad (29)$$

We model the threefold differential decay distribution including resonance and nonresonance contributions as follows:

$$\frac{d^3\Gamma}{dq^2 dp^2 d\cos\theta_K} = \frac{N(q^2)|\vec{q}'||\vec{p}'_K|}{8(2\pi)^5 m_B^2\sqrt{p^2}}[|e^{-i\delta}\tilde{H}_\perp + H_\perp^{nr}|^2$$
$$+ |e^{-i\delta}\tilde{H}_\parallel + H_\parallel^{nr}|^2 + |e^{-i\delta}\tilde{H}_0$$
$$+ H_0^{nr} + e^{-i\delta}\tilde{H}_0'|^2]. \quad (30)$$

Here, we included δ, a relative strong phase. There is just a single phase for all transversity amplitudes because all individual form factors can be chosen real valued and by approximate universality of the low recoil region. In view of other uncertainties we do not consider δ depending on q^2, because one expects the phase to only slowly vary with q^2. However, δ should vary with p^2. In neglecting this effect, which, in principle, could be taken care of, the strong phase becomes an effective p^2-bin averaged phase.

We stress that (30) is a model, with model parameter δ. Alternative descriptions would include modified Breit-Wigner propagators for the K^* and $B \to K^*$ form factors that take into account finite width effects. The model (30) can be improved by data, for instance, by measurements of the line shape outside the K^* signal region; see Fig. 5.
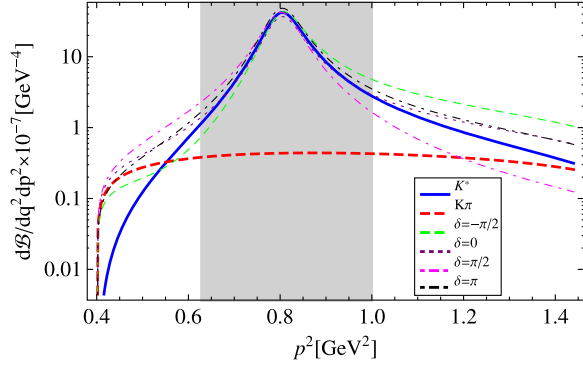
FIG. 5. Line shapes of the resonant K^* contribution (solid blue line), purely nonresonant contribution (dashed red line), and the line shapes which also include interference effects for different values of the strong phase $\delta = 0, \pm\pi/2, \pi$ at $q^2 = 16$ GeV^2. The (gray) shaded region corresponds to the P cut in p^2; cf. (25).

Furthermore, δ can be constrained from measurements of the ratios of angular coefficients in the process $B \to K^* \ell^+ \ell^-$, e.g., I_7/I_5, I_7/I_6; see Eq. (14) in [17] for the complete list and more details. These angular coefficients are not observable in the dineutrino mode. The benefit of using these ratios, as opposed to the total rate, lies in their independence on short-distance physics in the limit in which the right-handed operator can be neglected. Note that the angular coefficients become sensitive to the relative strong phase only in the p^2 region below and above the signal region (P cut); see [17]. Data on these coefficients exist at present only for the signal region [45].

The nonresonant amplitudes can be expanded in terms of orthonormal functions of the angle θ_K, resulting in a distribution that is more complicated than (18), which arises solely from vector and scalar meson states. Once higher waves $\ell \geq 2$ are present, the definition of the angular observables F_L and $A_{FB(L)}^K$ becomes more subtle. Here we use the projections via associated Legendre polynomials $P_0^0 = 1$, $P_1^0 = \cos\theta_K$, $P_2^0 = 1/2(3\cos^2\theta_K - 1)$ as

$$\frac{d\Gamma_L}{dq^2} = \int_{-1}^{1} \frac{d^2\Gamma}{dq^2 d\cos\theta_K}\left(\frac{1}{3}P_0^0 + \frac{5}{3}P_2^0\right)d\cos\theta_K, \quad (31)$$

$$b(q^2, p^2) = \int_{-1}^{1} \frac{d^2\Gamma}{dq^2 dp^2 d\cos\theta_K}\frac{3}{2}P_1^0 d\cos\theta_K, \quad (32)$$

from which $\langle F_L \rangle$ and $A_{FB(L)}^K$ follow as in Eqs. (22) and (24), respectively. In the limit in which only $\ell = 0$ and $\ell = 1$ effects are accounted for, one can insert the distribution (18) into the above formula to recover (21). Consequently, b probes predominantly S, P-wave interference.

To illustrate the effect of the nonresonant amplitudes we present in Fig. 6 the contributions to the branching fraction and $\langle F_L \rangle$, integrated over the high q^2 region, as functions of the strong phase and normalized to the pure K^* case. We find that the resulting uncertainty in the branching fraction is significant and can reach up to 20% in the P cut, while in $\langle F_L \rangle$ it is smaller, at most at the level of 2.5%.

We quantify the effect of the nonresonant contributions at high q^2 on the branching ratio in the last two rows of Table I. The corresponding central value and the first errors are the same as the corresponding entries for the resonant contributions (two rows above). The second errors are the result of the variation of the parameters of the nonresonant form factors (including the strong phase δ) via uniform distributions, while keeping all other inputs fixed to their central values. The upper and lower errors represent the maximal and minimal distances from the central value. The corresponding predictions for F_L are given in last row of Table II.

In Fig. 7 we show $A_{FB\,L}^K$ for different values of the strong phase δ. Other numerical input is fixed to central values. While in $A_{FB\,L}^K$ the Wilson coefficients $C_{L,R}$ drop out in the $\ell = 0, 1$ limit, there is a residual dependence from the interference of the K^* resonance with the D-wave components of the nonresonant amplitude. We checked that this effect is much smaller than the dependence on the strong
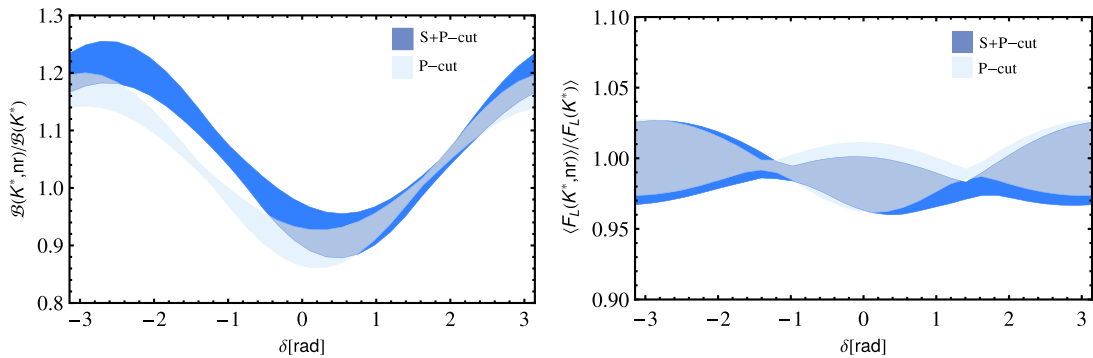

FIG. 6. Plot on the left: the ratio of $B \to (K^* + \mathrm{nr})(\to K\pi)\nu\bar{\nu}$ to $B \to K^*(\to K\pi)\nu\bar{\nu}$ in high-q^2-integrated branching fractions as a function of the relative strong phase δ. Plot on the right: the same for F_L. We fixed the $B \to K^*$ form factors and other parametric inputs to their central values and varied the parameters in the nonresonant form factors via uniform distributions. The boundaries of the bands correspond to minimal and maximal values obtained in this way. The darker and lighter blue bands correspond to P and $(S + P)$ cuts (25), respectively.
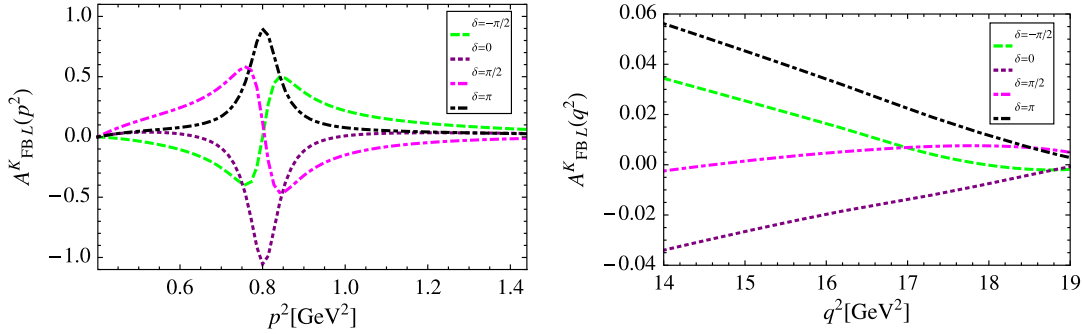
FIG. 7.   The forward-backward asymmetry $A_{\mathrm{FB}\,L}^{K}$ obtained using (32) as a function of p^2 after high q^2 integration (plot to the left) and as a function of q^2 after $S + P$-cut integration (plot to the right) for different phases $\delta = 0, \pm\pi/2, \pi$ and other input parameters fixed to central values. In each plot the longitudinal rate (31) is integrated over the high q^2 region and over p^2 within the $(S + P)$ cut (25).

phase δ, which allows one to experimentally constrain δ. Note that the corresponding uncertainties from the $B \to K^*$ form factors are between 5%–8%, while the nonresonant form factors introduce additionally $\sim 15\%$. Already a rough determination of δ would significantly reduce the uncertainties in the $B \to K^*(\to K\pi)\nu\bar{\nu}$ branching fraction; see Fig. 6.

Although presently there is no theory prediction available for nonresonant decays at low q^2, $A_{\mathrm{FB(L)}}^{K}$ can be studied here experimentally as well to constrain the (nonresonant) backgrounds also in this region.

V. CONCLUSIONS

We revisited the decay $B \to K^*\nu\bar{\nu}$, its virtues, and its uncertainties. $B \to K^*\nu\bar{\nu}$ data on F_L can be used, unlike $B \to K^*\ell^+\ell^-$ decays, in the entire q^2 region to test $B \to K^*$ form factors from lattice QCD or other non-perturbative means in a model-independent way if right-handed currents can be neglected. The latter can be tested, for instance, using null tests of the $B \to K^*\ell^+\ell^-$ angular distribution. The plot to the right in Fig. 1 illustrates the current level of form factor uncertainties. Probing form factors is limited by the resonant and nonresonant contributions considered in this work. They need to be taken into account once the K^* is treated beyond the narrow-width approximation.

We analyzed (i) finite width effects of the K^*, (ii) the effects induced by nonresonant contributions in the region of low hadronic recoil (high q^2), and (iii) contributions from scalar resonances decaying to $K\pi$ at low q^2. The restrictions to the kinematic regions in (ii) and (iii) originate from the current availability of $B \to K\pi$ and $B \to (K_0^*, \kappa)$ form factors, respectively.

Our findings are summarized in Tables I and II. At high q^2 the nonresonant contributions in the model (30) introduce an uncertainty of $\mathcal{O}(0.1)$ in the branching ratio, and at around a few percent in the longitudinal polarization fraction F_L. It is desirable to check these predominantly interference-induced effects with either a global analysis of

rare decay data or further theoretical study. On the other hand, the contributions of the scalar resonances to the branching ratio in the low q^2 region are small with respect to other sources of uncertainty and are at most of the order of 1% in the signal region (P cut) and $\lesssim 4\%$ for the wider $S + P$ cut. Their effect on F_L is negligible compared to the uncertainties from the $B \to K^*$ form factors.

The uncertainties in these backgrounds can be reduced with better knowledge of the form factors and line shapes. At high q^2 contributions from the 1430 family of higher kaon resonances are in addition kinematically suppressed. For nonresonant contributions at low q^2 presently no theoretical calculation is available. The new observable $A_{\mathrm{FB}\,L}^{K}$ (24) and (32) shown in Figs. 4 and 7, respectively, which arises from interference between the K^* and the background amplitudes, can be used to experimentally constrain hadronic backgrounds efficiently irrespective of the underlying short-distance model.

Because of the narrower width and absence of prominent low mass $\bar{s}s$ scalars decaying to KK, the backgrounds in $B_s \to \Phi(\to KK)\nu\bar{\nu}$ decays are smaller than in $B^0 \to K^*(\to K\pi)\nu\bar{\nu}$ decays. The problem of finite width-related backgrounds may of course be avoided altogether with the decay $B \to K\nu\bar{\nu}$, which, however, allows one to measure only its differential decay rate proportional to $f_+^2(q^2)|C_L + C_R|^2$.

There clearly is feedback from $b \to s\nu\bar{\nu}$ to $b \to s\ell^+\ell^-$ transitions and back: these modes are related by form factors and other hadronic input, as well as by Wilson coefficients in $SU(2)_L$-symmetric SM extensions. On the other hand, the dineutrino modes are not polluted by electromagentic effects, and they do probe flavor physics in a complementary way; notably, third generation leptons are included and may shed light on ongoing and future tests of lepton universality.

APPENDIX A: POLARIZATION VECTORS

Our conventions for the metric and Levi-Cività tensors are $g_{\mu\nu} = \text{diag}(1, -1, -1, -1)$ and $\epsilon_{0123} = 1$, respectively. The choice of the polarization vectors of the neutrino pair in the B-rest frame is given by

$$\tilde{\epsilon}^\mu_\pm = \frac{1}{\sqrt{2}}(0, \mp 1, i, 0), \qquad \tilde{\epsilon}^\mu_0 = \frac{1}{\sqrt{q^2}}(|\vec{q}|, 0, 0, q_0),$$

$$\tilde{\epsilon}^\mu_t = \frac{1}{\sqrt{q^2}}(q^0, 0, 0, |\vec{q}|), \qquad (A1)$$

while the components of the four-vector $q^\mu = (q^0, 0, 0, |\vec{q}|)$, with $|\vec{q}| = \sqrt{\lambda(m_B^2, q^2, m_{K^*}^2)}/(2m_B)$. The polarization vectors satisfy the conditions of orthogonality and completeness, respectively,

$$\tilde{\epsilon}^{*\mu}_m \tilde{\epsilon}_{\mu m'} = g_{mm'}, \qquad \sum_{m,m'} \tilde{\epsilon}^{*\mu}_m \tilde{\epsilon}^\nu_{m'} g_{mm'} = g^{\mu\nu}. \quad (A2)$$

The direction of the z axis is opposite to the direction of motion of the K^* in the B-rest frame. Polarization vectors of the K^* meson in this frame read

$$\epsilon^\mu_\pm = \frac{1}{\sqrt{2}}(0, \pm 1, i, 0), \quad \epsilon^\mu(0) = \frac{1}{m_{K^*}}(k_z, 0, 0, k_0), \quad (A3)$$

where $k_z = -|\vec{q}|$. These satisfy the orthogonality and completeness relations

$$\epsilon^{*\mu}_m \epsilon_{\mu m'} = -\delta_{mm'}, \quad \sum_{m,m'} \epsilon^{*\mu}_m \epsilon^\nu_{m'} \delta_{mm'} = -g^{\mu\nu} + \frac{k^\mu k^\nu}{m_{K^*}^2}, \quad (A4)$$

where the indices $m = 0, 1, 2, 3$ are ordered as $m = t; 0, \pm$, respectively.

APPENDIX B: FORM FACTORS

The matrix elements of the vector and axial currents $\bar{s}\gamma_\mu(\gamma_5)b$ between the B and the K^* mesons with polarization n are parametrized with the standard form factors $V(q^2)$ and $A_{0,1,2}(q^2)$,

$$\langle K^*(k, n)|\bar{s}\gamma_\mu b|B(p_B)\rangle = \epsilon_{\mu\nu\alpha\beta}\epsilon^{*\nu}_n p_B^\alpha k^\beta \frac{2iV(q^2)}{m_B + m_{K^*}},$$

$$\langle K^*(k, n)|\bar{s}\gamma_\mu\gamma_5 b|B(p_B)\rangle = -\epsilon^*_{n\mu}(m_B + m_{K^*})A_1(q^2)$$

$$+ (p_{B\mu} + k_\mu)\frac{\epsilon^*_n \cdot q}{m_B + m_{K^*}}A_2(q^2)$$

$$+ q_\mu(\epsilon^*_n \cdot q)\frac{2m_{K^*}}{q^2}$$

$$\times (A_3(q^2) - A_0(q^2)), \quad (B1)$$

where

$$A_3(q^2) = \frac{m_B + m_{K^*}}{2m_{K^*}}A_1(q^2) - \frac{m_B - m_{K^*}}{2m_{K^*}}A_2(q^2). \quad (B2)$$

The matrix element for the final state scalar reads

$$\langle K_0^*(k)|\bar{s}\gamma_\mu\gamma_5 b|B(p_B)\rangle = (p_B + k)_\mu f_+(q^2) + q_\mu f_-(q^2). \quad (B3)$$

The form factors for $B \to K_0^*(1430)$ are calculated within QCD sum rules (QCDSR) [33]. In our numerical analysis we use QCDSR form factors which are parametrized as [33]

$$f_i(q^2) = \frac{f_i(0)}{1 - a_i(q^2/m_B^2) + b_i(q^2/m_B^2)^2}, \quad (B4)$$

where a_i, b_i for $i = +, -$ are fit coefficients. In the limit of vanishing lepton masses only $f_+(q^2)$ contributes. The corresponding parameters are $f_+(0) = 0.31 \pm 0.08$, $a_+ = 0.81$, and $b_+ = -0.21$ [33].

APPENDIX C: NUMERICAL INPUT

In Table III we collect the numerical values of the inputs used in this paper.

TABLE III. Numerical values of the inputs.

Parameter	Value	Source
$|V_{ts}^* V_{tb}|$	0.0401 ± 0.0010	[41]
$\alpha_e(m_b)$	$1/127.925(16)$	[26]
$\Gamma(B_0)$	$(4.333 \pm 0.020) \times 10^{-13}$ GeV	[26]
$\Gamma(B_s)$	$(4.342 \pm 0.032) \times 10^{-13}$ GeV	[26]
$m_{K_0^*}$	1425 ± 50 MeV	[26]
$\Gamma_{K_0^*}$	270 ± 80 MeV	[26]
m_κ	$658(13)$ MeV	[27]
Γ_κ	$557(24)$ MeV	[27]
$|g_\kappa|$	$[0\ldots0.2]$	[13]
$\arg g_\kappa$	$[\pi/2\cdots\pi]$	[13]
f_π	130.4 ± 0.2 MeV	[26]
f_K	156.2 ± 0.7 MeV	[26][a]
f_{B_d}	188 ± 4 MeV	[42]
f_{B_s}	224 ± 5 MeV	[42]
g	0.569 ± 0.076	[43,44][a]

[a]Uncertainties added in quadrature.

[1] T. Blake, T. Gershon, and G. Hiller, Annu. Rev. Nucl. Part. Sci. **65**, 113 (2015).

[2] T. Blake, G. Lanfranchi, and D. M. Straub, Prog. Part. Nucl. Phys. **92**, 50 (2017).

[3] T. Aushev *et al.*, arXiv:1002.5012.

[4] P. Urquijo, Report No. BELLE2-MEMO-2016-008.

[5] J. Grygier *et al.* (Belle Collaboration), arXiv:1702.03224.

[6] P. Colangelo, F. De Fazio, P. Santorelli, and E. Scrimieri, Phys. Lett. B **395**, 339 (1997).

[7] G. Buchalla, G. Hiller, and G. Isidori, Phys. Rev. D **63**, 014015 (2000).

[8] W. Altmannshofer, A. J. Buras, D. M. Straub, and M. Wick, J. High Energy Phys. 04 (2009) 022.

[9] M. Bartsch, M. Beylich, G. Buchalla, and D.-N. Gao, J. High Energy Phys. 11 (**2009**) 011.

[10] A. J. Buras, J. Girrbach-Noe, C. Niehof,f, and D. M. Straub, J. High Energy Phys. 02 (2015) 184.

[11] J. Girrbach-Noe, arXiv:1410.3367.

[12] C. Niehoff, *Proc. Sci.*, EPS-HEP2015 (2015) 553 [arXiv:1510.04582].

[13] D. Becirevic and A. Tayduganov, Nucl. Phys. **B868**, 368 (2013).

[14] J. Matias, Phys. Rev. D **86**, 094024 (2012).

[15] T. Blake, U. Egede, and A. Shires, J. High Energy Phys. 03 (2013) 027.

[16] D. Das, G. Hiller, M. Jung, and A. Shires, J. High Energy Phys. 09 (2014) 109.

[17] D. Das, G. Hiller, and M. Jung, arXiv:1506.06699.

[18] R. Aaij *et al.* (LHCb Collaboration), J. High Energy Phys. 11 (2016) 047.

[19] J. F. Kamenik and C. Smith, Phys. Lett. B **680**, 471 (2009).

[20] G. Buchalla and A. J. Buras, Nucl. Phys. **B548**, 309 (1999).

[21] M. Misiak and J. Urban, Phys. Lett. B **451**, 161 (1999).

[22] J. Brod, M. Gorbahn, and E. Stamou, Phys. Rev. D **83**, 034030 (2011).

[23] A. Bharucha, D. M. Straub, and R. Zwicky, J. High Energy Phys. 08 (2016) 098.

[24] C. Hambrock, G. Hiller, S. Schacht, and R. Zwicky, Phys. Rev. D **89**, 074014 (2014).

[25] R. R. Horgan, Z. Liu, S. Meinel, and M. Wingate, *Proc. Sci.*, LATTICE2014 (2015) 372 [arXiv:1501.00367].

[26] J. Beringer *et al.* (Particle Data Group Collaboration), Phys. Rev. D **86**, 010001 (2012).

[27] S. Descotes-Genon and B. Moussallam, Eur. Phys. J. C **48**, 553 (2006).

[28] P. del Amo Sanchez *et al.* (*BABAR* Collaboration), Phys. Rev. D **83**, 072001 (2011).

[29] M. Döring, U. G. Meißner, and W. Wang, J. High Energy Phys. 10 (2013) 011.

[30] C. D. Lu and W. Wang, Phys. Rev. D **85**, 034014 (2012).

[31] R. Aaij *et al.* (LHCb Collaboration), J. High Energy Phys. 12 (2016) 065.

[32] S. Prelovsek, L. Leskovec, C. B. Lang, and D. Mohler, Phys. Rev. D **88**, 054508 (2013).

[33] T. M. Aliev, K. Azizi, and M. Savci, Phys. Rev. D **76**, 074017 (2007).

[34] D. Becirevic, S. Fajfer, I. Nisandzic, and A. Tayduganov, arXiv:1602.03030.

[35] C. Hambrock and G. Hiller, Phys. Rev. Lett. **109**, 091802 (2012).

[36] U. G. Meißner and W. Wang, J. High Energy Phys. 01 (2014) 107.

[37] R. R. Horgan, Z. Liu, S. Meinel, and M. Wingate, Phys. Rev. D **89**, 094501 (2014).

[38] C. L. Y. Lee, M. Lu, and M. B. Wise, Phys. Rev. D **46**, 5040 (1992).

[39] B. Bajc, S. Fajfer, R. J. Oakes, and T. N. Pham, Phys. Rev. D **58**, 054009 (1998).

[40] G. Buchalla and G. Isidori, Nucl. Phys. **B525**, 333 (1998).

[41] M. Bona *et al.* (UTfit Collaboration), J. High Energy Phys. 10 (2006) 081.

[42] R. J. Dowdall, C. T. H. Davies, R. R. Horgan, C. J. Monahan, and J. Shigemitsu (HPQCD Collaboration), Phys. Rev. Lett. **110**, 222003 (2013).

[43] J. M. Flynn, P. Fritzsch, T. Kawanai, C. Lehner, C. T. Sachrajda, B. Samways, R. S. Van de Water, and O. Witzel, *Proc. Sci.*, LATTICE2013 (2014) 408 [arXiv:1311.2251].

[44] J. M. Flynn, P. Fritzsch, T. Kawanai, C. Lehner, C. T. Sachrajda, B. Samways, R. S. Van de Water, and O. Witzel (RBC and UKQCD Collaborations), Phys. Rev. D **93**, 014510 (2016).

[45] R. Aaij *et al.* (LHCb Collaboration), J. High Energy Phys. 02 (2016) 104.